In-situ growth of Zn-based Metal-Organic Frameworks in ultra-high surface area nano-wood aerogel for efficient CO_2 capture and separation

Jianpeng Huang[a], Deshi Yang[a], Zhipeng Hu[a], Huihui Zhang[a], Zhijun Zhang[a]*, Fengqiang Wang[a], Yanjun Xie[a], Shouxin Liu[a], Qingwen Wang[b], Charles U. Pittman Jr.[c]

[a] Key Laboratory of Biobased Material Science and Technology (Ministry of Education), Northeast Forestry University, Harbin 150040, PR China

[b] Collage of Materials and Energy, South China Agricultural University, Guangzhou 510642, PR China

[c] Department of Chemistry, Mississippi State University, Mississippi State, MS 39762, USA

SUPPORTING INFORMATION

Table of Contents

1. Materials

Natural Balsa wood used in this study was purchased from SINOKINO materials company (China). The samples were cut into 10 × 10 × 10 (mm) cubes. Zinc nitrate hexahydrate $Zn(NO_3)•6H_2O$(98 %), 2,5-dihydroxyterephthalic acid (dhtp, > 98%), 2-methylimidazole (2-MeIm, > 99%), 2-aminobenzimidazole (BMI-NH_2, > 97%), benzimidazole (BMI, > 98%), N, N- dimethyl- formamide (DMF, ≥99.8 %), dimethylacetamide (DMAc, ≥ 99.8 %), acetone (AR), methanol (≥ 99 %), ethanol (≥ 99 %), sodium chlorite ($NaClO_2$, 80%), sodium hypochlorite (NaClO, 10%), 2,2,6,6-tetramethylpiperidin-1-yloxy (TEMPO) and lithium chloride (LiCl, ≥ 99%) were purchased from Aladdin Shanghai China. LiCl was dried at 120 °C in vacuum overnight before use. Other reagents were used without further purification.

2. Experimental Section

2.1 Preparation of Delignified Wood (DW)

The synthesis of DW used here was reported elsewhere.[1] In a typical procedure, wood blocks were cooked in 2 wt% aqueous sodium chlorite with acetate buffer solution (pH 4.6) at 95 °C for 12 h. Each wood block dimension was 10 × 10 × 10 mm. Subsequently, the blocks were washed with deionized water several times to remove excess chemicals.

2.2 Preparation of TEMPO-oxidized regenerated wood (TRW) templates

The wet DW blocks obtained in the previous step were immersed in ethanol for water exchange 30 min thrice, followed by immersion in DMAc for 30 min thrice and then overnight. Then the wood blocks were immersed in 8 wt% LiCl / DMAc solution at 30 °C for 8 h to dissolve the wood cell wall partially. Then, the blocks were quickly immersed into acetone for at least 8 h to regenerate the nanocellulose aerogel within the regenerated wood (RW), and the RW blocks were repeatedly washed with deionized water. Next, the RW blocks were oxidized with a TEMPO/NaClO/$NaClO_2$ at 60 °C and pH 6.8 for 48 h. After TEMPO-mediated oxidation, wood blocks were washed repeatedly using a 50% aqueous ethanol solution to remove residual chemicals. The washed samples were designated TRW.

2.3 Fabrication of TRW/Z-74

$Zn(NO_3)•6H_2O$ (5 mmol) was dissolved in 50 ml of deionized water to obtain solution A. Then, 2.23

mmol of 2, 5-dihydroxyterephthalic acid was dissolved in 50 ml of 0.4M aqueous NaOH (solution B). Wet TRW samples (1 g dry mass) were next immersed in solution A for ion exchange procedures at room temperature for 6 h. To promote more Zn^{2+} to bind with cellulosic carboxyl groups, the TRW blocks in solution A were placed inside a vacuum drying oven at room temperature where they were held 30 min at 0.04 MPa and then transferred to ambient pressure for 30 min. This procedure was repeated at least 3 times to complete the ion exchange. Then, solution B was slowly decanted into solution A and stirred at 200 rpm for 12 h at 25 °C. After 12 h, the wood blocks were carefully removed from the mixed solution, and repeatedly washed with methanol. Finally, TRW/Z-74 was obtained after drying with supercritical CO_2. Zn-MOF-74 powder was also obtained from this reaction. After removing TRW/Z-74, the mother liquor was centrifuged at 8000 rpm, and the collected products were washed with fresh methanol at least three times. Zn-MOF-74 was obtained by solvent removal under vacuum at 120 °C overnight.

2.4 Fabrication of TRW/Z-7N

The previous ion exchange step was repeated by immersing the wet TRW samples (1 g dry mass) in 50 ml DMF solution containing 5 mmol $Zn(NO_3)•6H_2O$. After contacting Zn^{2+} with the carboxyl groups on the cellulose for 6 h at 25 °C, a well dispersed 50 ml methanol solution of the organic linkers (7 mmol 2-aminobenzimidazole and 3 mmol benzimidazole) was quickly poured into the Zn^{2+} solution containing the TRW blocks and reacted for 8 h at 25 °C. Then the TRW blocks were removed, and unreacted organic linkers on the surfaces' were removed by fresh methanol. Finally, drying with supercritical CO_2 produced the TRW/Z-7N. Pristine ZIF-7-NH_2 was also isolated from this reaction. The remaining MOF solution after removing TRW/Z-7N was centrifuged (8000 rpm, 15 min), and the collected products were methanol washed several times and dried at 120 °C overnight.

2.5 Fabrication of TRW/Z-8N

$Zn(NO_3)•6H_2O$ (5 mmol) was dissolved in 50 mL of methanol. Then the as-prepared wet TRW samples (1 g dry mass) were added. The previous ion exchange steps were then repeated. Thereafter, 50 ml of methanol solution containing 12.5 mmol of dissolved 2-methylimidazole and 10 mmol of 2-aminobenzimidazole were added into the Zn^{2+} solution while stirring (200 rpm) for 12 h. After reaction, unreacted organic linkers on the TRW surface were washed away with fresh methanol.

Finally, the TRW/Z-8N samples were obtained and dried with supercritical CO_2. The corresponding pristine ZIF-8-NH_2 MOF was obtained by centrifugation (8000 rpm, 15 min) of the methanol solution from the TRW/ZIF-8-NH_2 preparation. The powder collected was cleaned with methanol several times and then dried at 120 °C overnight.

2.6 Fabrication of TRW/M-MOF-74 (M=Mg^{2+}, and Co^{2+})

TRW/M-MOF-74 (M=Mg^{2+}, and Co^{2+}) was synthesized using the identical method described above except that $Zn(NO_3)$•$6H_2O$ was replaced by an equimolar quantity of $Mg(NO_3)$•$6H_2O$ or $Co(NO_3)$•$6H_2O$. Pristine $Mg(NO_3)$•$6H_2O$ or $Co(NO_3)$•$6H_2O$ was also isolated from this reaction. The remaining MOF solution after removing TRW/MOFs was centrifuged (8000 rpm, 15 min), and the collected products were methanol washed several times and dried at 120 °C overnight.

3. Characterization Section

3.1 Material characterization

The composites' microscopic morphologies were observed using a field emission scanning electron microscope (FE-SEM, Apreo) at an accelerating voltage of 5 kV. The samples' cross-sections were first trimmed with a sliding microtome (Leica sm2010 R, Germany) and longitudinal sections were cut with a sharp knife, then directly observed. Fourier transform infrared spectra (FT-IR) were recorded by a Nicolet 6700 with ATR mode over a scan range of 4000 to 500 cm^{-1}. The samples' crystal structures were studied by X-ray Diffraction (XRD, SHIMADZU 6100) using copper Kα radiation (λ = 1.5406Å). TRW/MOFs were cut into slices of 1 cm both in length and width and 1 mm in thickness for XRD. The diffraction data were obtained in 5°/min angular steps at a counting time of 0.24s per step and recorded in the range of 2θ = 5-35°. Thermal stability data for composites and pure MOFs were collected using a thermogravimetric analyzer (TG, 209F1) using 5-10 mg samples heated from 30°C to 800°C under Ar at a ramp rate of 10 K/min. The surface elemental composition and chemical state of the materials were studied using X-ray photoelectron spectroscopy (XPS, Thermo Scientific k-alpha). All binding energies were calibrated using C 1s with a binding energy of 284.8 eV. The mechanical properties of TRW/MOF composites were evaluated by compression tests performed on a universal testing machine (Suns, UTM2503). A 10 KN load cell with a strain rate of 10%/min, 23°C and 50% relative humidity were used. The dimensions of all specimens were 10 ×10

×10 mm (tangential x radial x axial). Young's modulus was evaluated by observing the slope of the initial linear region of the stress-strain curve. The yield point (σp), indicates the stress at which structural collapse occurs. At the yield point, plastic deformation begins and the material is no longer able to recover elastically. The yield strength was defined as the stress at the intersection between the tangent of the elastic region and the tangent of the platform region. The Zn content in the composites was measured by inductively coupled plasma luminescence spectroscopy (ICP-OES, Optima 8300). A dry sample (0.1 g) was hydrolyzed with 72% (w/w) H_2SO_4 prior to measurement. The composite specific surface areas were analyzed by N_2 adsorption/desorption isotherms measured using ASAP 2460 at 77 K. The pore capacity and pore distribution were analyzed by density inverse function theory (DFT). The samples (~ 100 mg) were degassed under vacuum at 100 °C for 12 h before measurement to remove water and residual solvents.

3.2 Calculation of crystallinity

The calculation of cellulose crystallinity in DW and TRW was done by the XRD peak intensity method[2] using equation (1):

$$CI = \frac{I_{200} - I_{am}}{I_{200}} \times 100\% \quad (1)$$

where CI represents the crystallinity index, I_{200}, and I_{am} represent the intensity of diffraction peak intensities at (200) and amorphous regions, respectively.

3.3 Loading content of MOFs on TRW.

The weight ratio of MOFs on the TRW was calculated using equation 2:

$$\text{Loading}\% = \frac{W_3 - W_2}{W_1 - W_2} \times 100\% \quad (2)$$

Where W_1, W_2, and W_3 represent the values of remaining weight percentages of pure MOFs, TRW, and TRW/MOF composites obtained from TG analysis, respectively.

3.3 Gas adsorption testing

CO_2 and N_2 adsorption isotherms of the composites and MOF powders were analyzed volumetrically using a Micromeritics ASAP 2460 adsorption apparatus. CO_2 adsorption isotherms were measured at two different temperatures (273 K, 298 K) up to 106 KPa (1.06 bar). The N_2 adsorption isotherm was measured at 298 K rising to 106 KPa (1.06 bar). Approximately 120 mg of sample was desorbed

under vacuum at 150 °C for 12 h to remove moisture and other organic small molecules from the sample. The CO_2 adsorption cycle test for TRW/Z-74 was also measured on the ASAP 2460 instrument. At the end of one cycle, the CO_2 was desorbed under vacuum at 60°C for 6 h. Afterwards, the above CO_2 adsorption experiments were repeated.

3.4 Isothermal heat of adsorption(ΔH_{ads}) calculation

The Clausius-Clapeyron equation (3) was used to calculate the ΔH_{ads} of the composites at 273 K and 298 K as follows:[3]

$$\ln(\frac{P_2}{P_1}) = -\frac{\Delta H_{ads}}{R}(\frac{1}{T_2} - \frac{1}{T_1}) \quad (3)$$

Where P_2, P_1 denote pressure; T_2, T_1 denote temperature; and R represents the gas constant.

3.5 Gas selectivity calculation

The CO_2/N_2 (15%/85%) selectivities of TRW/MOFs were calculated by ideal solution adsorption theory (IAST).[4] The molar fraction of each component in the adsorbed phase was calculated using equation 4:

$$\int_{t=0}^{py_1/x_1} F_1(t)d\ln t = \int_{t=0}^{py_2/x_2} F_2(t)d\ln t \quad (4)$$

Where t is a dummy variable, x_i is the molar fraction of component i in the adsorbed phase, y_i is the molar fraction of component i in the gas phase, F_i is the adsorption isotherm function of the pure component, and p is the total pressure.

The CO_2 and N_2 adsorption isotherms of TRW/MOFs were fitted by a Double-Site Langmuir (DSL) model (equation 5):

$$Q = \frac{q_1 b_1 p}{1 + b_1 p} + \frac{q_2 b_2 p}{1 + b_2 p} \quad (5)$$

Where Q is the total amount adsorbed (mmol/g), q_1, q_2 represent the saturation capacity (mmol/g), b_1, b_2 represent the Langmuir parameter and p represents the pressure (KPa).

Equation (6) was used to determine the amount adsorbed in the gas mixture:

$$\frac{1}{n_t} = \frac{x_1}{n_1} + \frac{x_2}{n_2} \quad (6)$$

Where n_t represents the total number of moles of adsorbent per unit mass in the adsorption phase, n_i (i=1, 2) represents the number of moles of adsorbent per unit mass in component. i is the number of

moles of adsorbent per unit mass in the adsorption phase.

The selectivity calculation is then performed by equation 7:

$$S = \frac{n_{CO_2} / n_{N_2}}{y_{CO_2} / y_{N_2}} \tag{7}$$

4. Figures

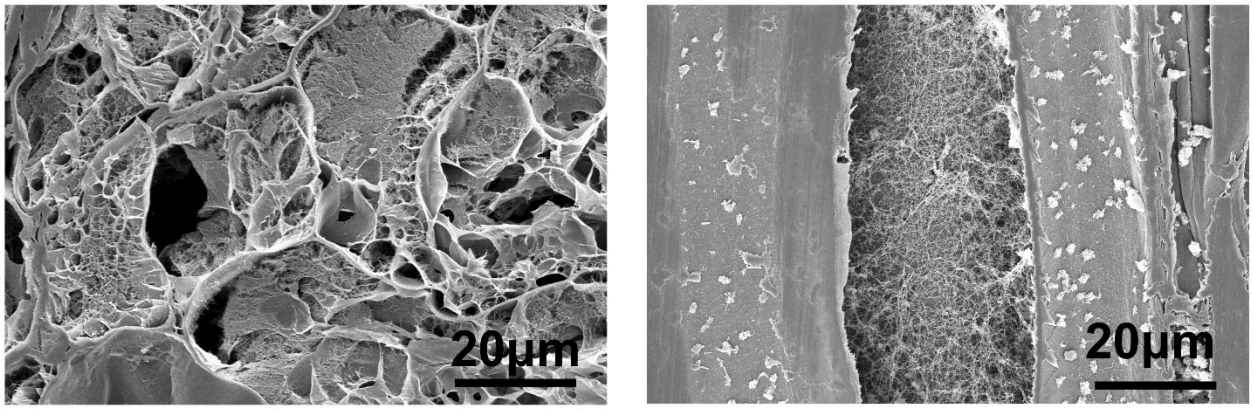

Fig. S1 a, FE-SEM image of regenerated wood cross-section and **b**, longitudinal section.

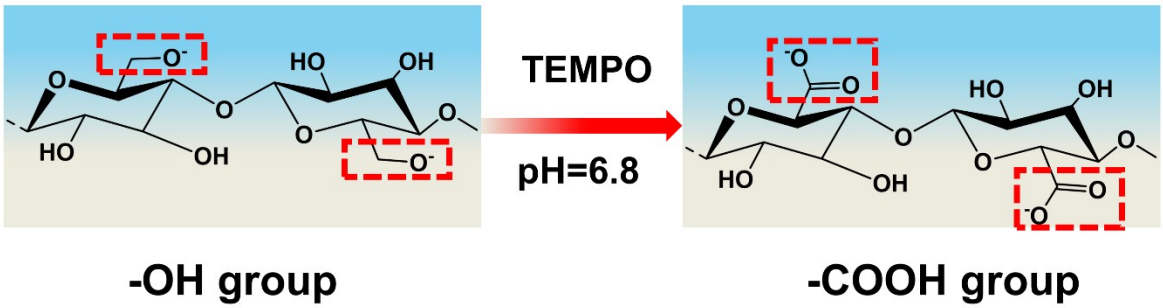

Fig. S2 Schematic illustration of transformation of hydroxyl groups to carboxy groups after TEMPO oxidization treatment.

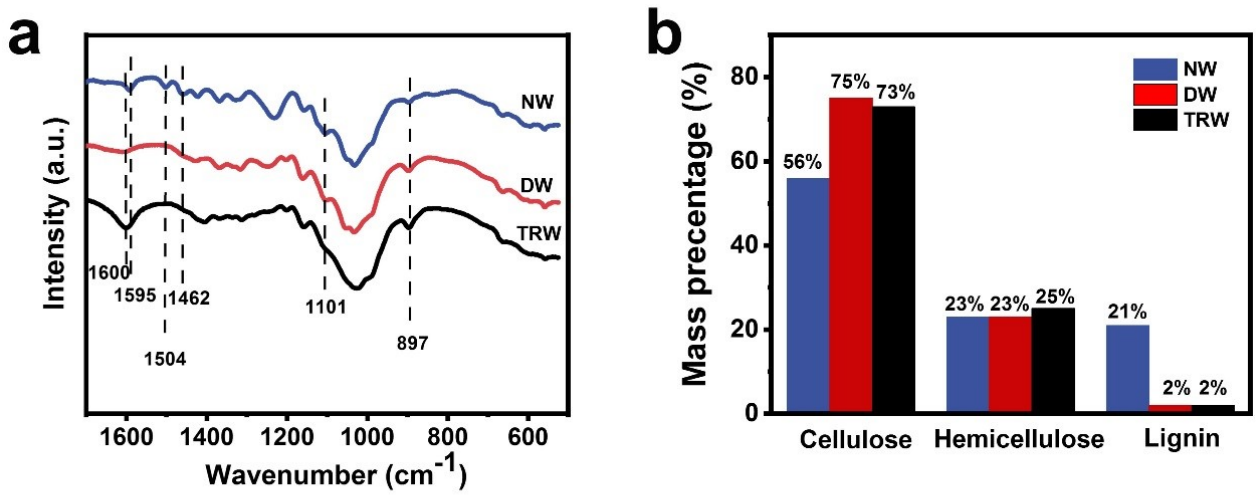

Fig. S3 a, FT-IR spectra and **b,** composition evolution of the natural wood (NW), delignified wood (DW) and TEMPO-regenerated wood (TRW).

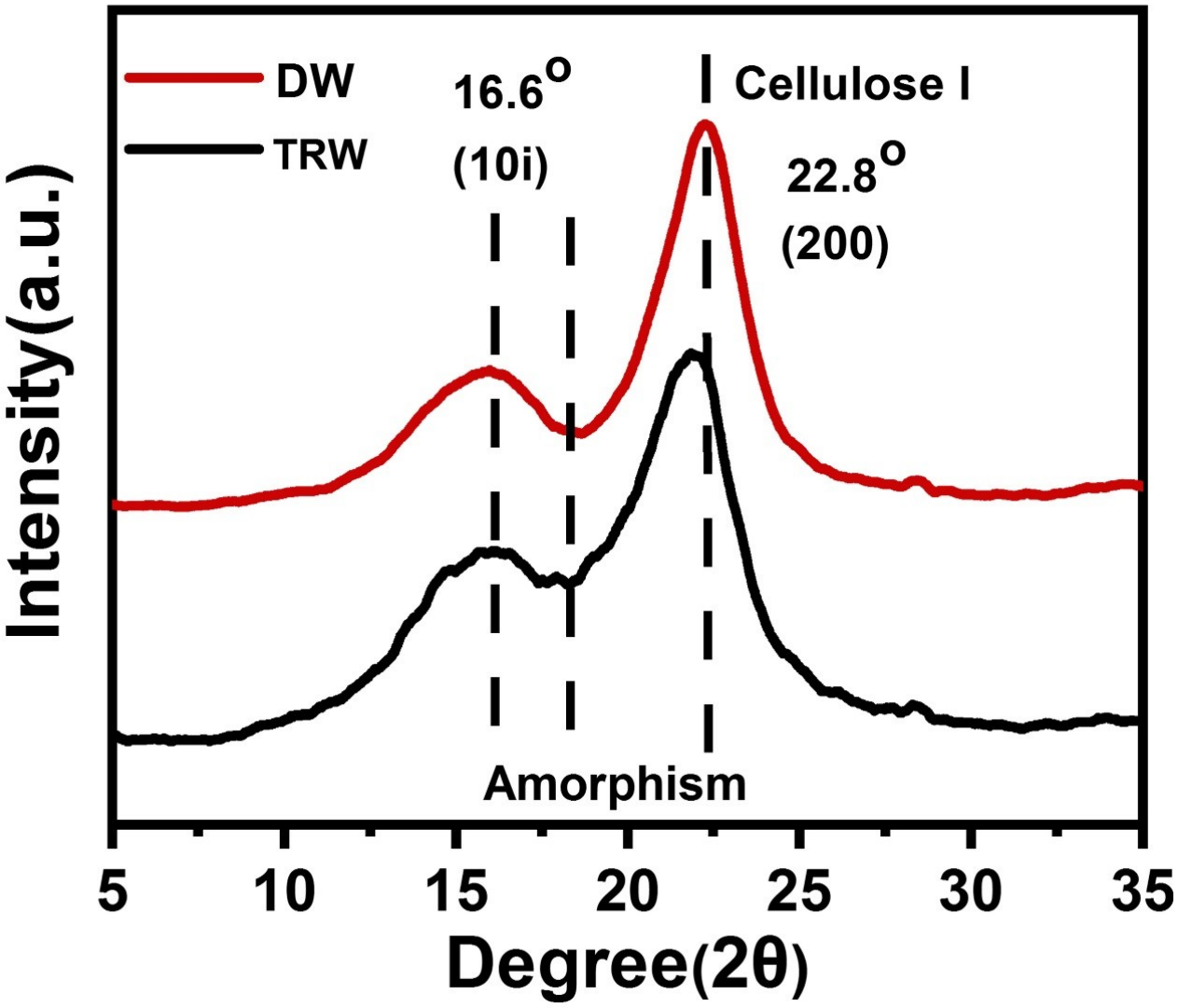

Fig. S4 XRD patterns of delignified wood (DW) and TEMPO-regenerated wood (TRW).

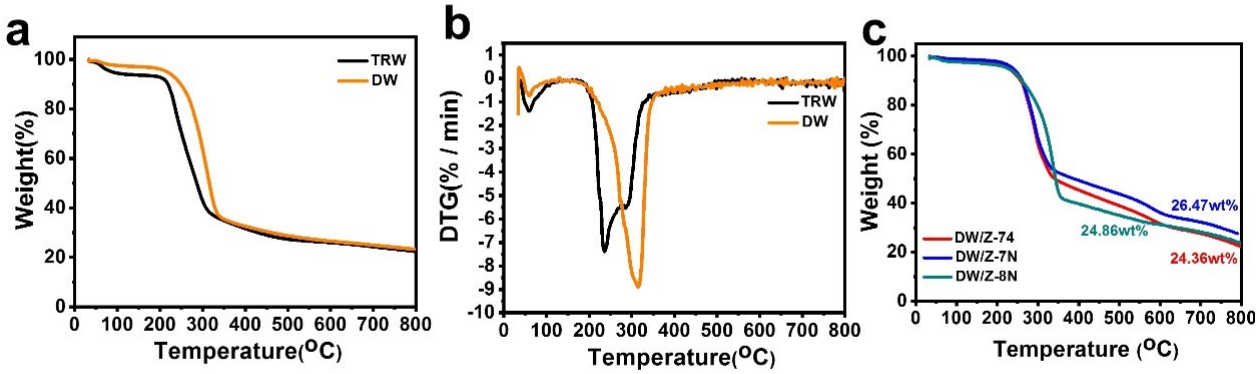

Fig. S5 a, Thermogravimetric curves and **b**, corresponding first derivative weight loss curves of TEMPO-regenerated wood (TRW), and delignified wood (DW). **c**, Thermogravimetric curves of DW/Z-74, DW/Z-7N, DW/Z-8N.

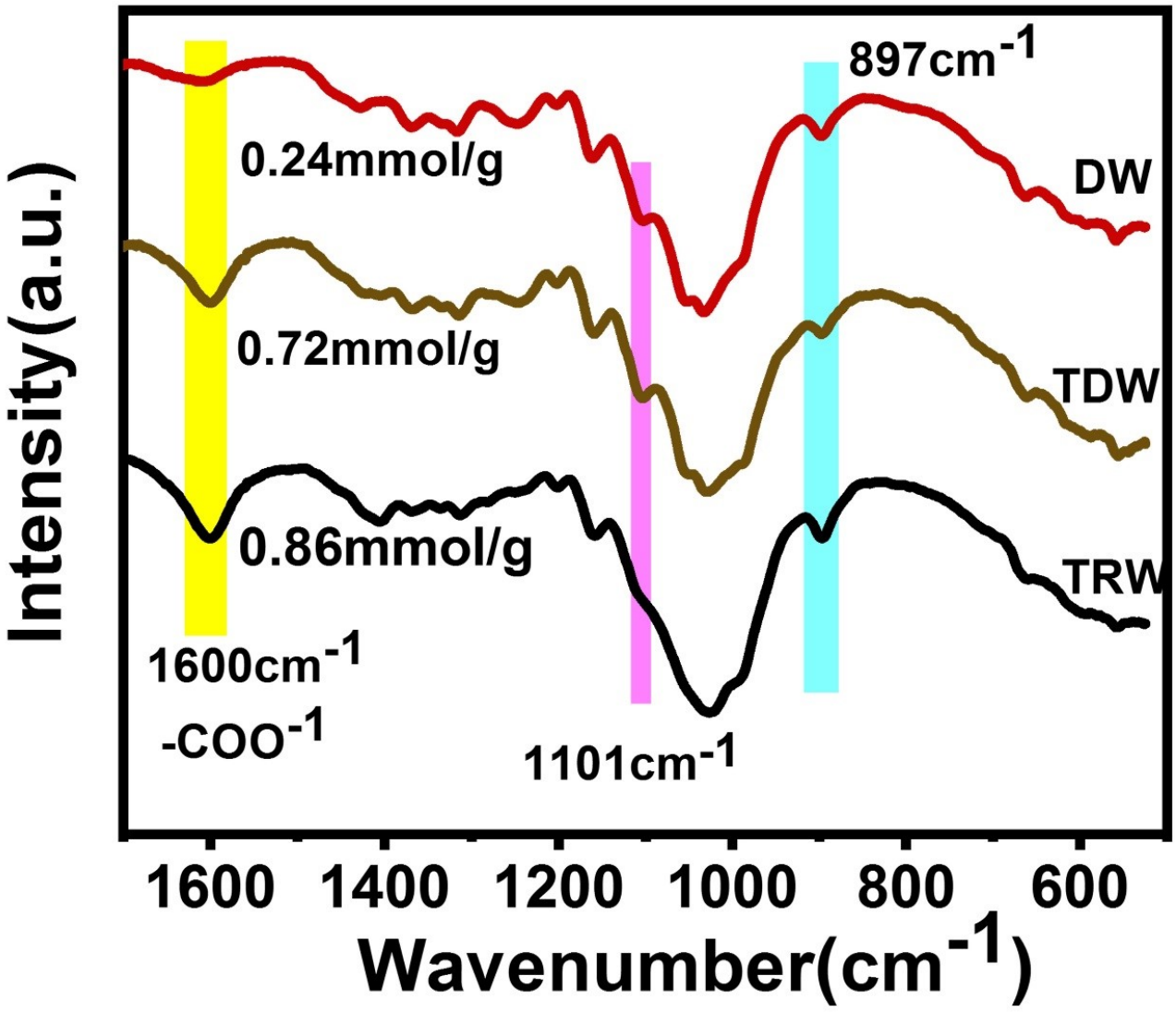

Fig. S6 FT-IR spectra and carboxyl contents of delignified wood (DW), TEMPO-delignified wood (TDW), and TEMPO-regenerated wood (TRW).

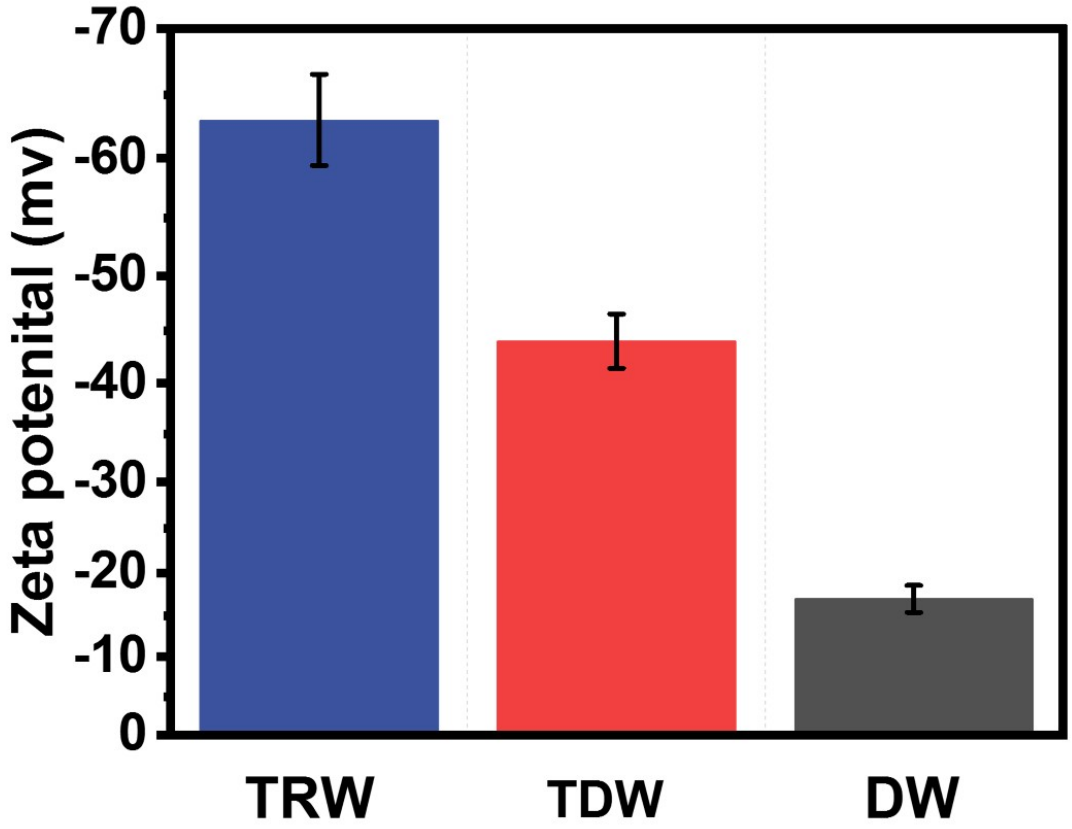

Fig. S7 Apparent Zeta potential of TEMPO-regenerated wood (TRW), TEMPO-delignified wood (TDW), and delignified wood (DW).

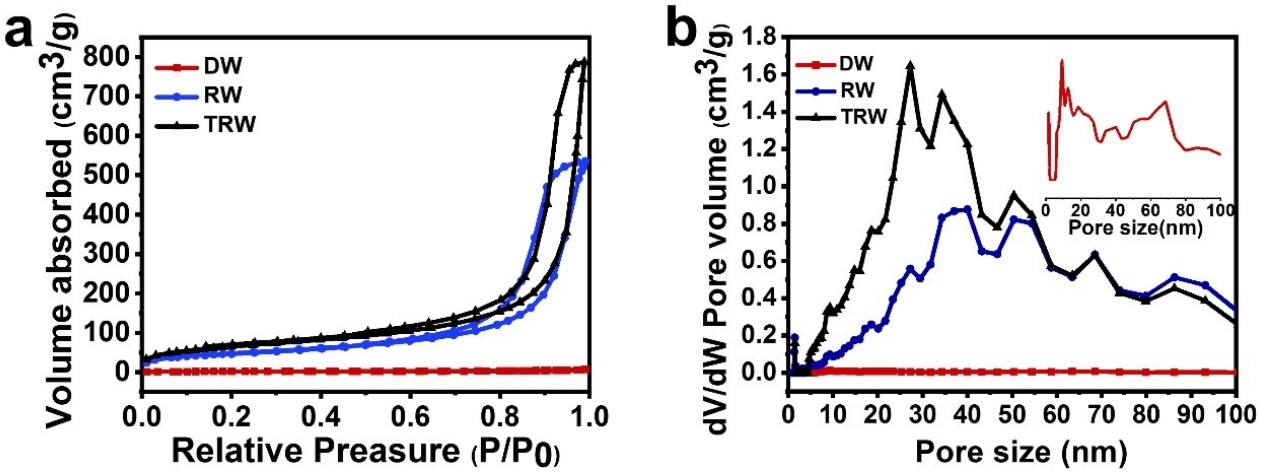

Fig. S8 a, N_2 adsorption/desorption isotherms of delignified wood (DW), regenerated wood (RW) and TEMPO-regenerated wood (TRW) and **b**, pore size distribution (PSD) curves of DW, RW and TRW.

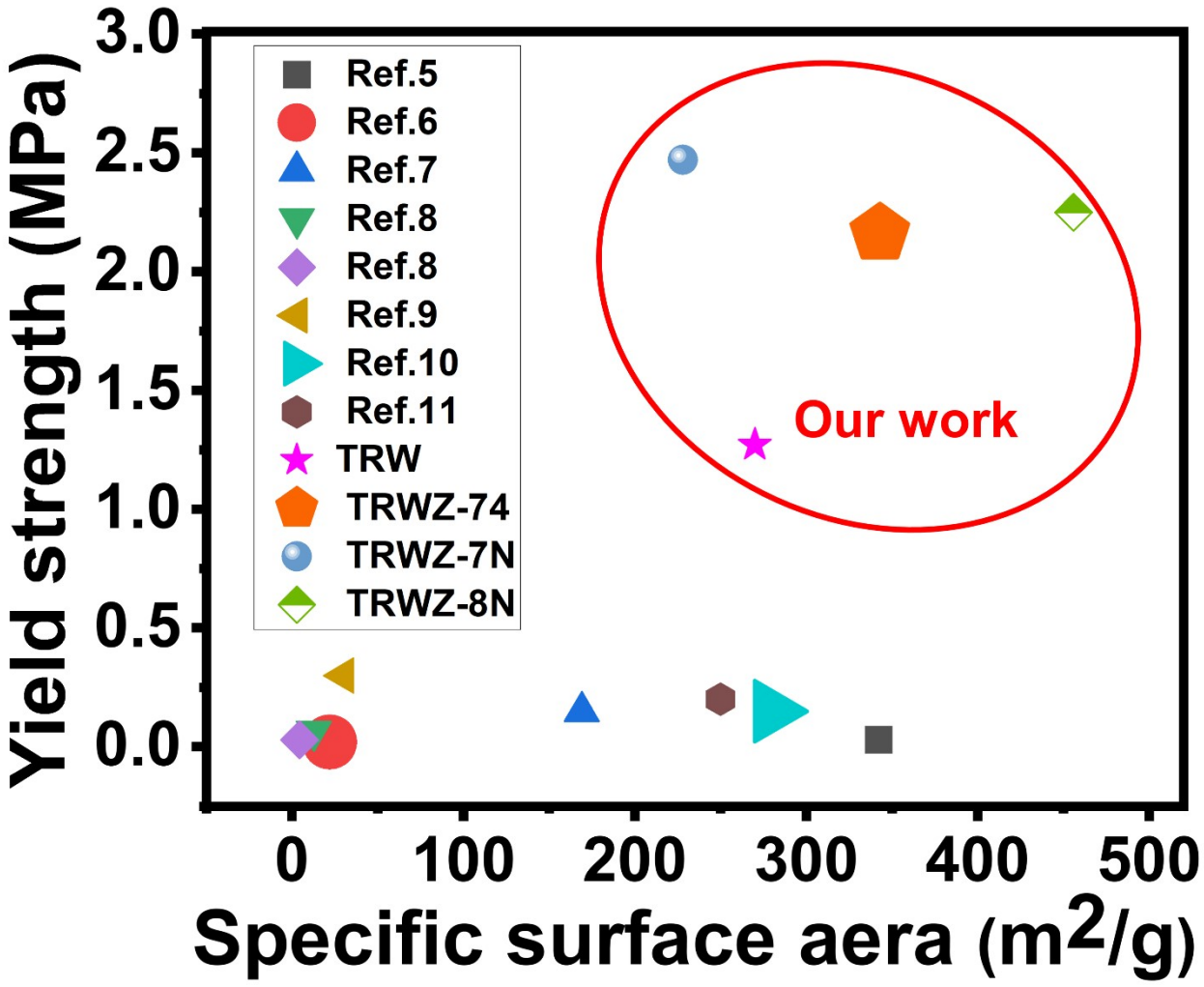

Fig. S9 Yield strength versus the specific surface area for documented cellulose-based aerogels and foams.[5-11]

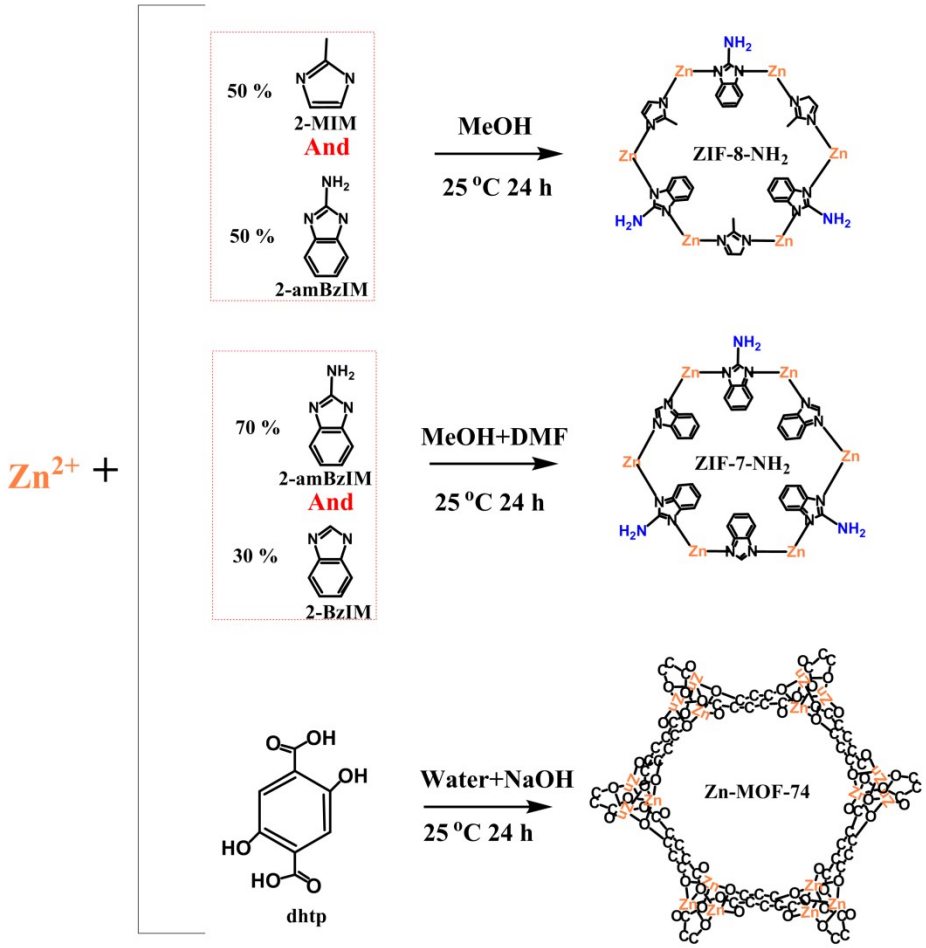

1

2 **Fig. S10** Synthesis scheme of pure MOFs.

3

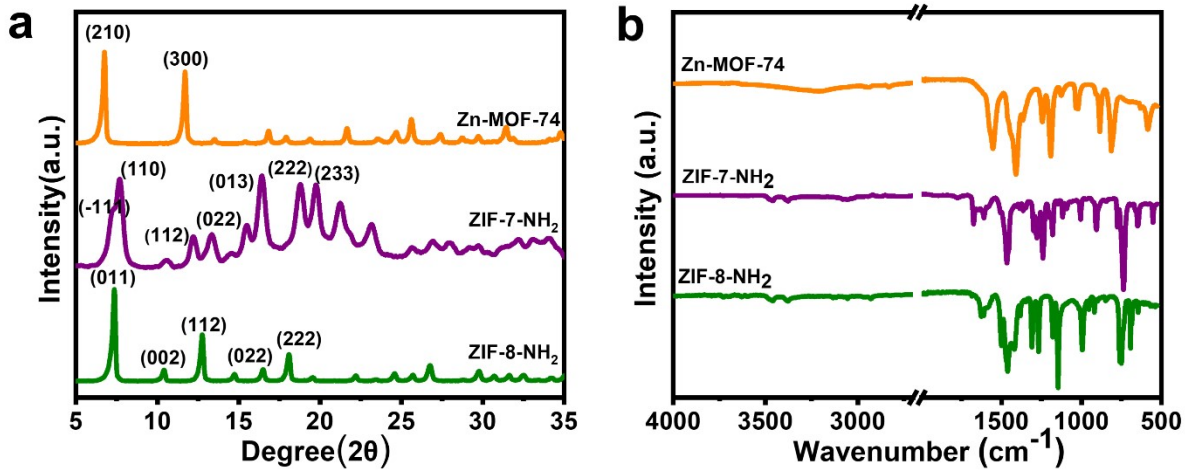

Fig. S11 a, XRD patterns and **b**, FTIR spectra of Zn-MOF-74, ZIF-7-NH_2, and ZIF-8-NH_2.

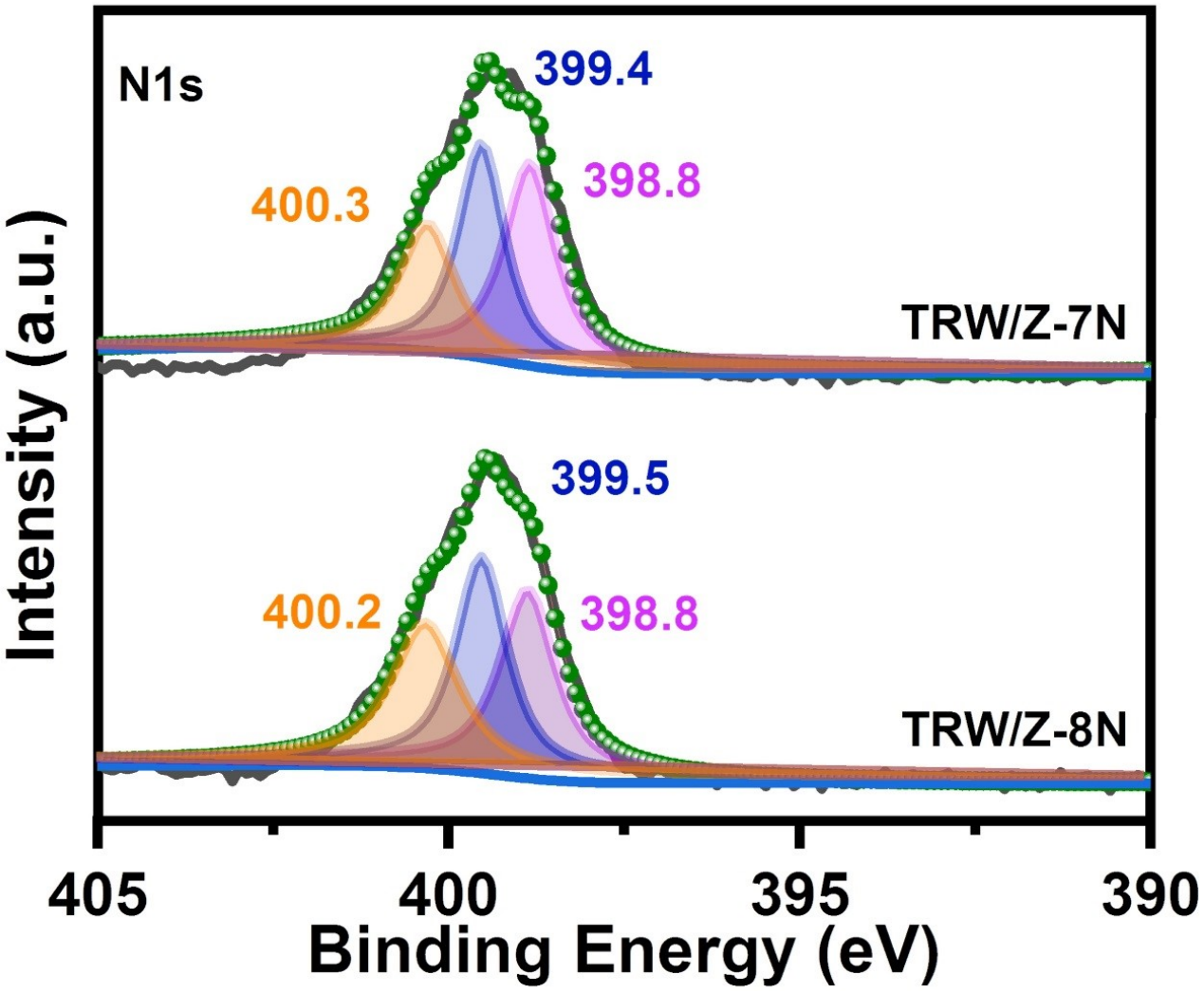

Fig. S12 High-resolution N1s XPS spectra of TRW/Z-7N and TRW/Z-8N.

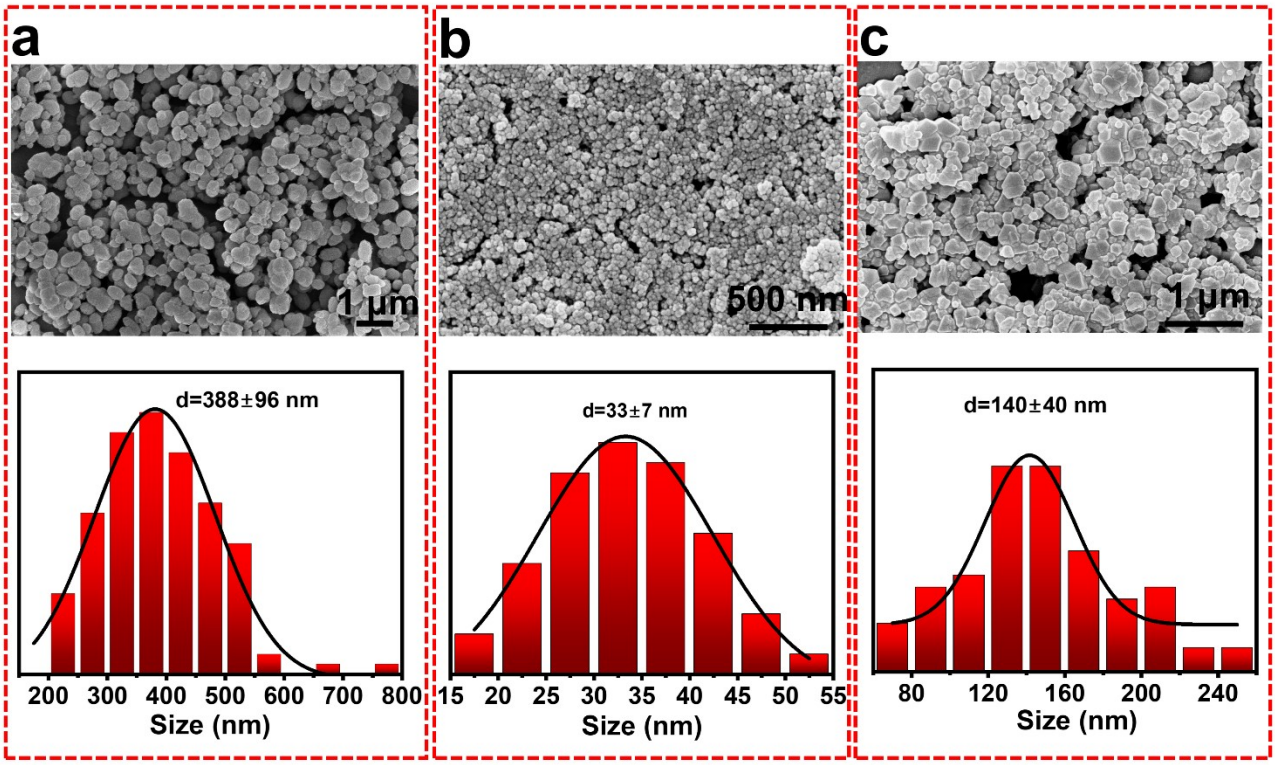

Fig. S13 SEM images and particle size distribution of **a.** Zn-MOF-74, **b.** ZIF-7-NH_2, **c.** ZIF-8-NH_2.

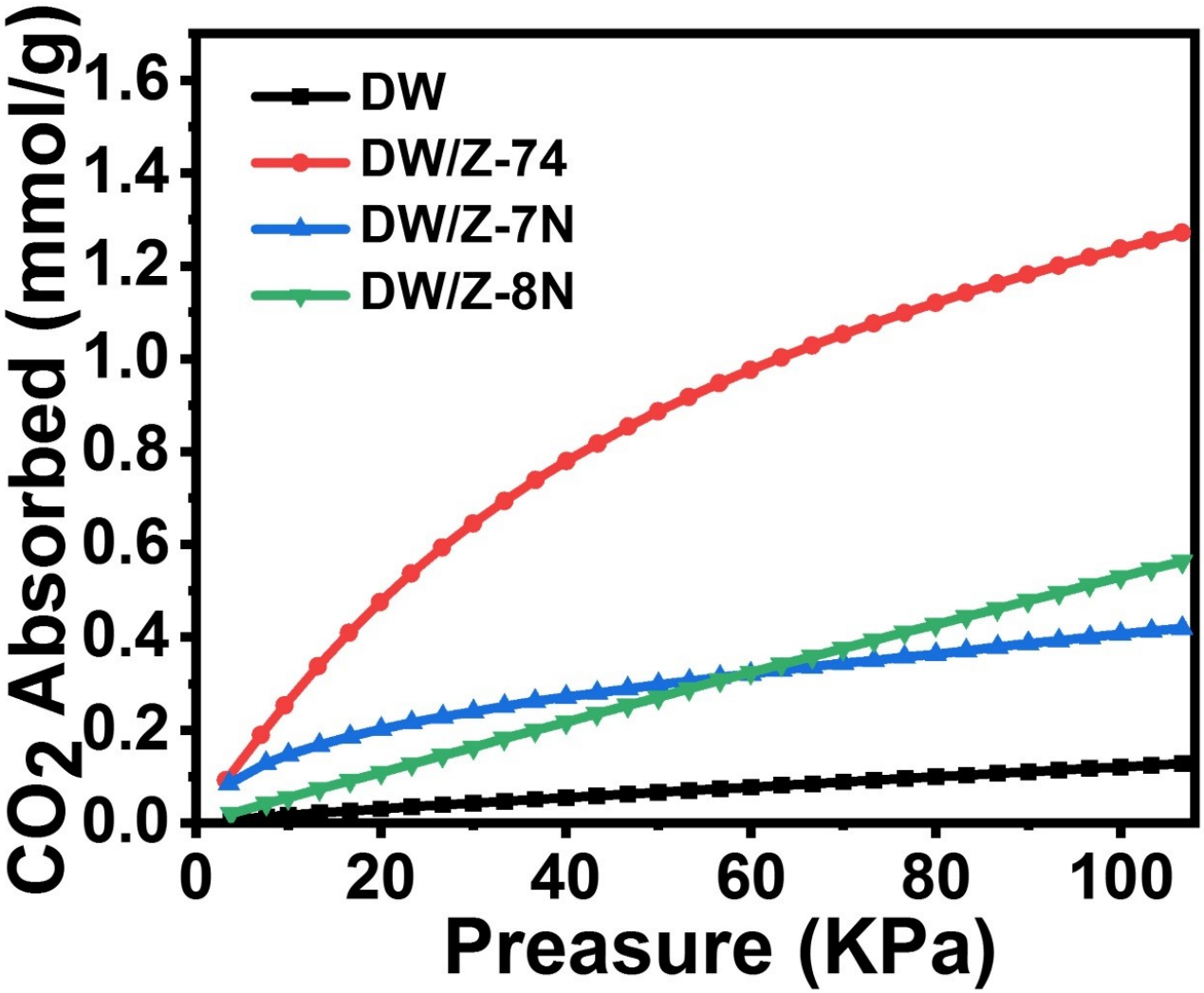

Fig. S14 CO_2 sorption isotherms of DW, DW/Z-74, DW/Z-7N, DW/Z-8N at 298 k, 106 KPa.

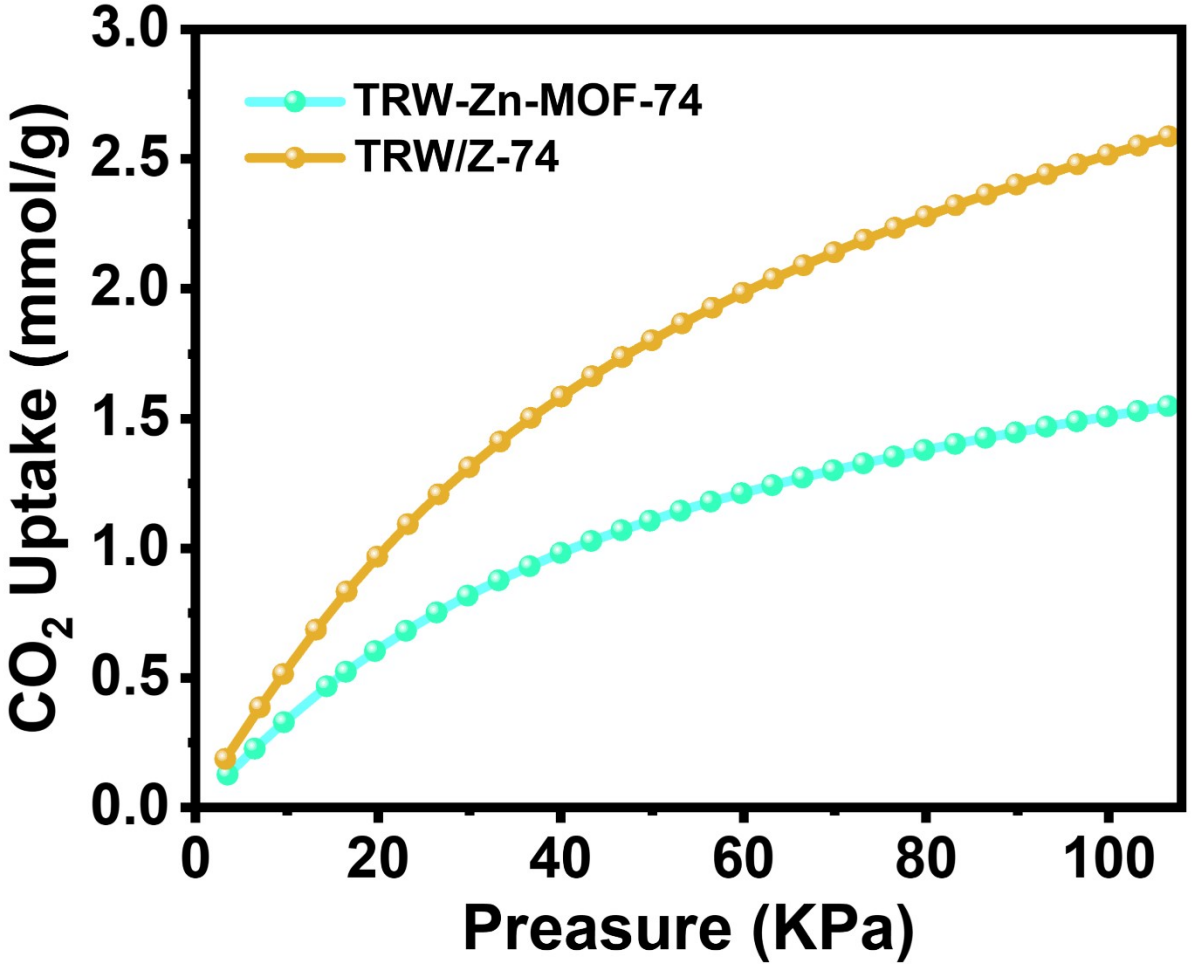

Fig. S15 CO_2 sorption isotherms of TRW-Zn-MOF-74 and TRW/Z-74 at 298 k, 106 KPa.

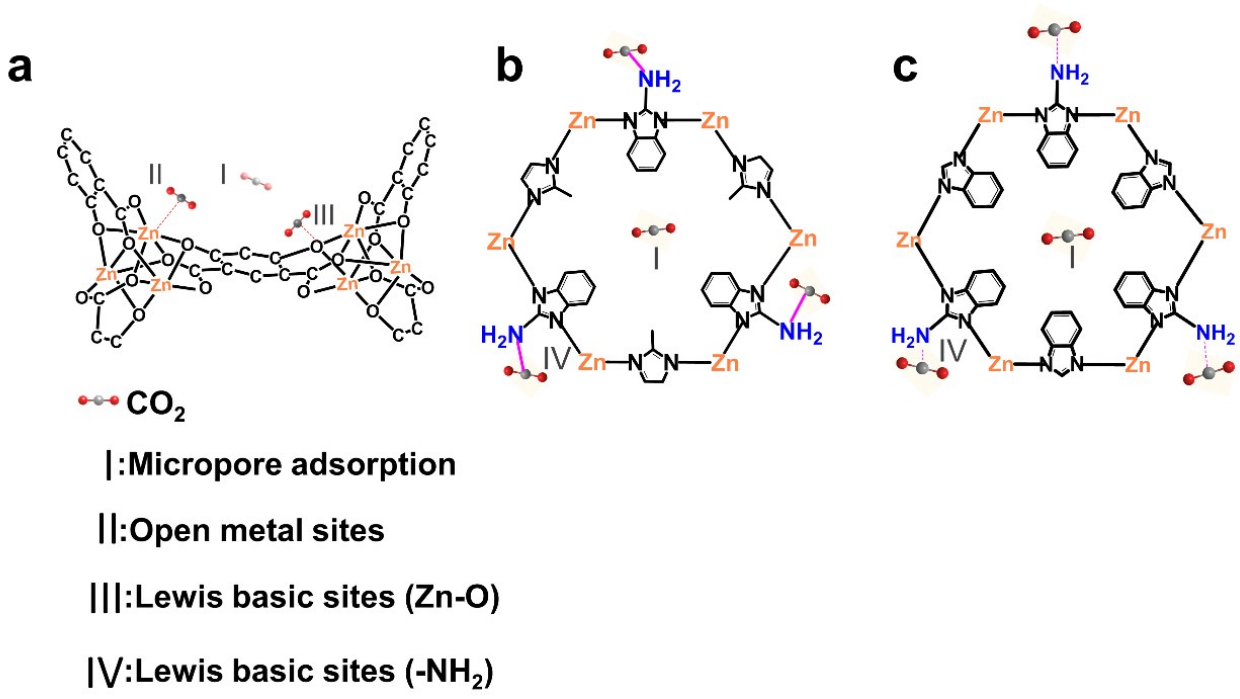

Fig. S16 Mechanism of CO_2 adsorption by a, Zn-MOF-74; b, ZIF-8-NH_2; c, ZIF-7-NH_2.

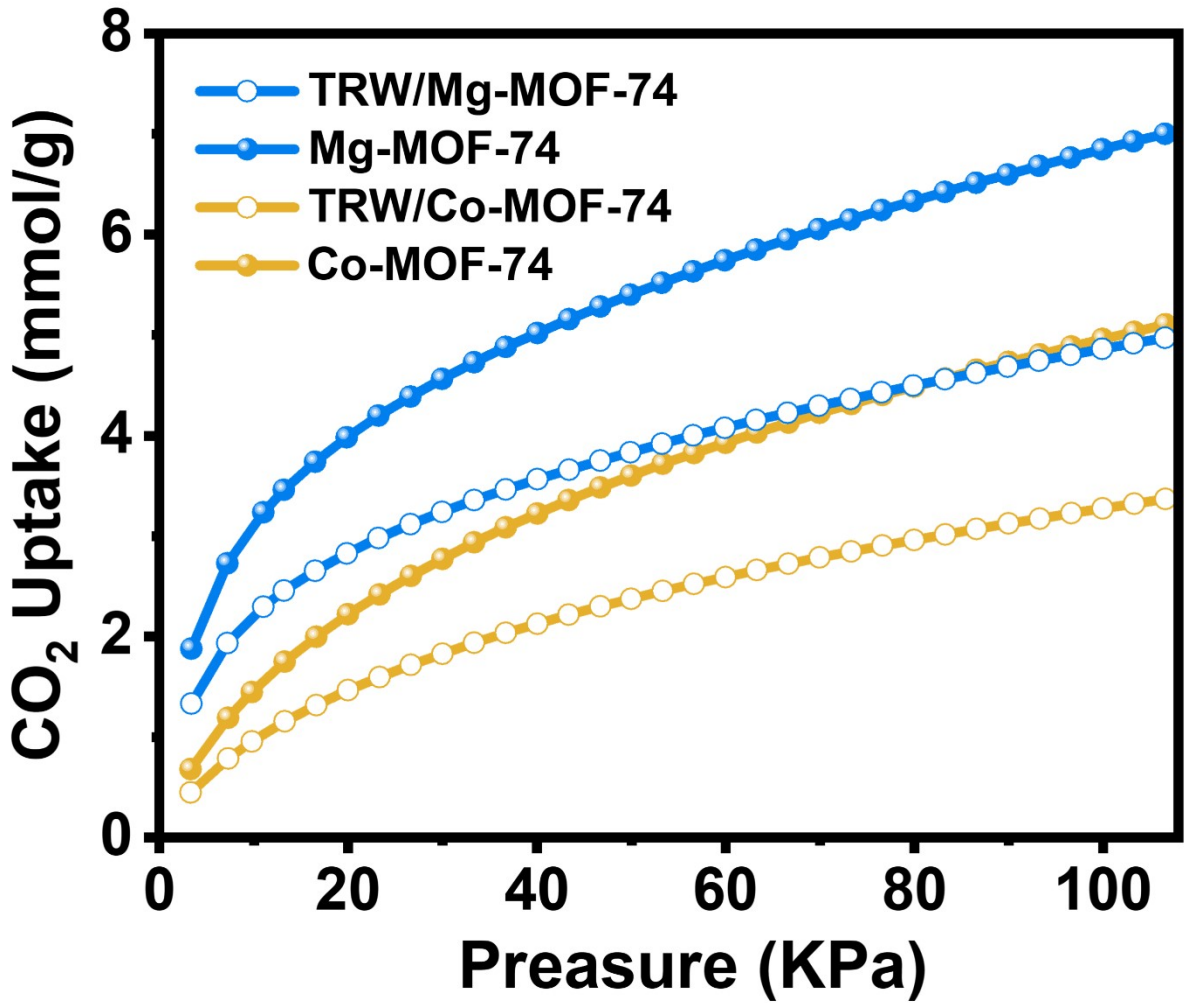

Fig. S17 CO_2 sorption isotherms of TRW/Mg-MOF-74, Mg-MOF-74, TRW/Co-MOF-74, and Co-MOF-74 at 298 k, 106 KPa.

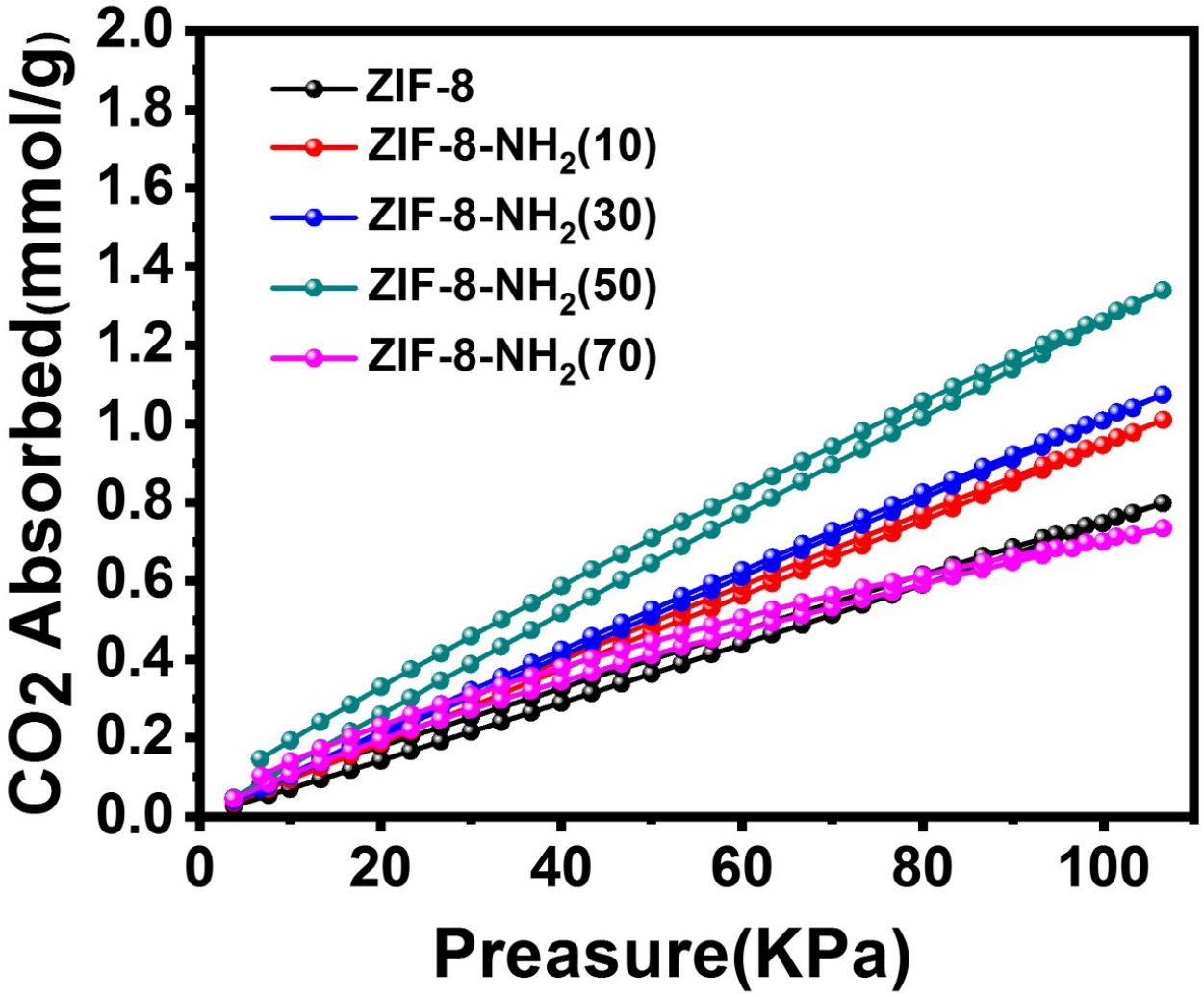

Fig. S18 CO_2 sorption isotherms of ZIF-8 and ZIF-8-NH_2(X), X=10, 30, 50, 70 at 298 k, 106 KPa.

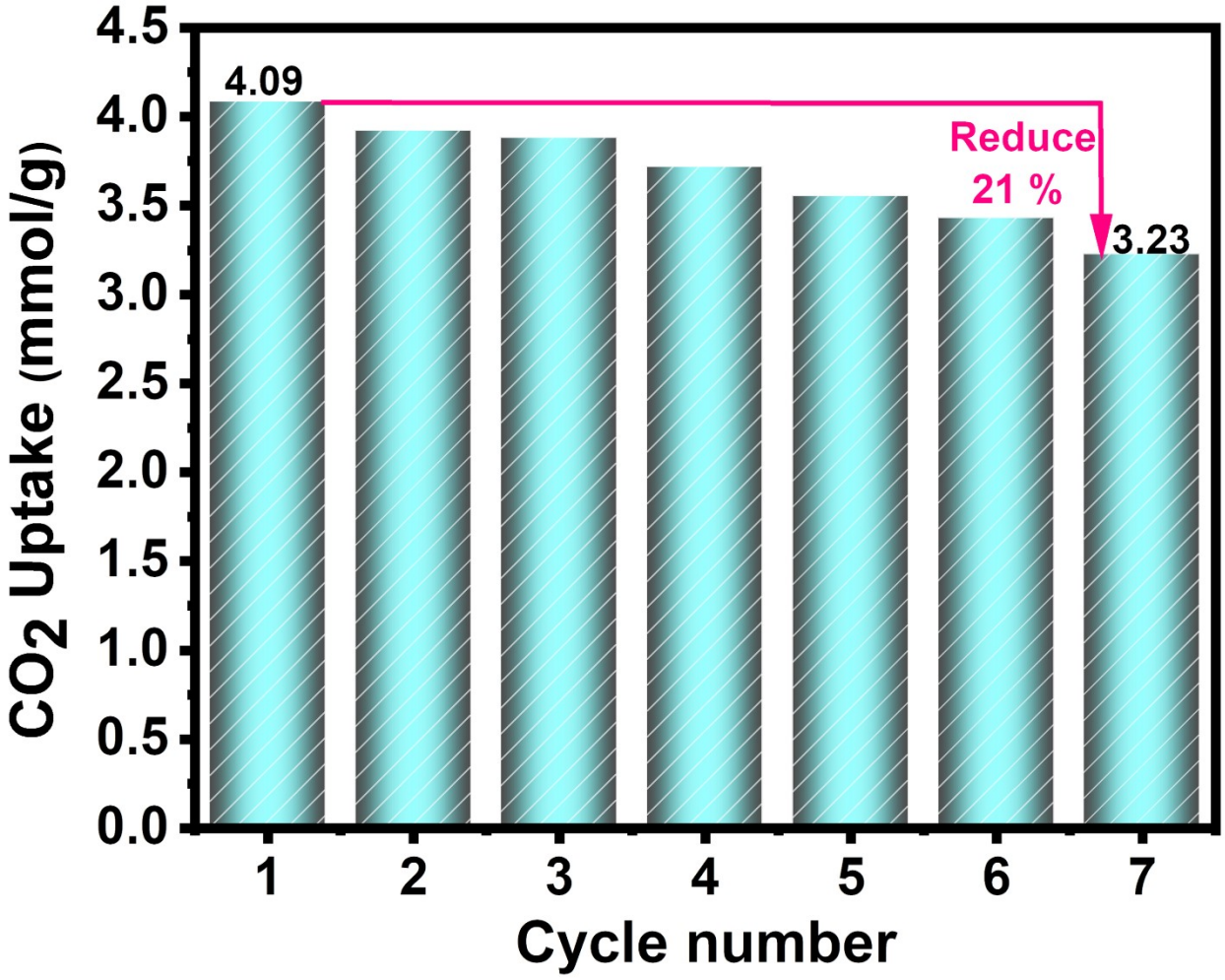

Fig. S19 CO_2 adsorption cycles over Zn-MOF-74 at 298 K, 106KPa.

5. Tables

Table S1 Specific surface areas, pore volumes, micropore volumes, CO_2 adsorption at 273K and 298K and isothermal heats of adsorption of TRW, RW, DW and TRW/MOF composites and their corresponding MOF powders

Samples	$S_{BET}(m^2/g)$	Pore volume (cm^3/g)	Micropore volume(cm^3/g)	CO_2 uptake (mmol/g) 273 K	CO_2 uptake (mmol/g) 298 K	ΔH_{ads} (KJ/mol)
TRW	270	1.02	0.0042	0.26	0.24	2.34
RW	184	0.61	0.0016	/	/	/
DW	5.6	0.01	0.0007	0.16	0.14	1.45
TRW/Z-74	343	0.43	0.12	3.42	2.59	28.13
TRW/Z-7N	228	0.80	0.033	0.92	0.86	19.57
TRW/Z-8N	456	0.70	0.15	1.44	1.34	11.89
Zn-MOF-74	702	0.38	0.26	5.64	4.09	30.87
ZIF-7-NH_2	406	0.79	0.09	1.47	1.31	24.83
ZIF-8-NH_2	833	0.56	0.37	2.47	2.27	14.75

Table S2 MOF contents of TRW/MOFs

	MOFs content (wt.%)
TRW/Z-74	35.53
TRW/Z-7N	41.15
TRW/Z-8N	37.44

Table S3 Density, Young's modulus and yield strength of TRW and TRW/MOF composites parallel

to the longitudinal axis[a]

Sample	Density(kg/m^3)	Young's modulus (MPa)	Yield strength (MPa)
TRW	81.37±4	26.43±5	1.27±0.10
TRW/Z-74	112.59±5	46.29±9	2.16±0.13
TRW/Z-7N	121.43±7	57.37±11	2.47±0.40
TRW/Z-8N	116.23±4	49.16±7	2.25±0.15

The values in parentheses are the sample standard deviations.

Table S4 Dual-site Langmuir (DSL) model (equation S5) parameters of TRW/MOF composites.

Parameters	TRW/Z-74		TRW/Z-7N		TRW/Z-8N	
	CO_2	N_2	CO_2	N_2	CO_2	N_2
q_1	-0.0214	-8.2293	0.1215	-0.0034	-0.0024	-0.0012
q_2	4.1413	1.7541	0.8992	0.2700	25.1540	0.4174
b_1	2.7389	1.2875	1.0275	-8.2188	4.6516	3.1620
b_2	0.0157	8.3958	0.0125	0.0043	5.0392	0.0022
R^2	0.9999	0.99947	0.9949	0.9979	0.9999	0.9989

6. Reference

1. H. Guan, Z. Cheng and X. Wang, *ACS nano*, 2018, **12**, 10365-10373.
2. U. P. Agarwal, S. A. Ralph, C. Baez, R. S. Reiner and S. P. Verrill, *Cellulose*, 2017, **24**, 1971-1984.
3. A. Kumar, D. G. Madden, M. Lusi, K. J. Chen, E. A. Daniels, T. Curtin, J. J. Perry IV and M. J. Zaworotko, *Angew. Chem., Int. Ed.*, 2015, **54**, 14372-14377.
4. S. Ga, S. Lee, G. Park, J. Kim, M. Realff and J. H. Lee, *Chem. Eng. J.*, 2021, **420**, 127580.
5. H. Sehaqui, M. Salajková, Q. Zhou and L. A. Berglund, *Soft Matter*, 2010, **6**, 1824-1832.
6. S. Xiao, R. Gao, Y. Lu, J. Li and Q. Sun, *Carbohydr. Polym.*, 2015, **119**, 202-209.
7. N. Pircher, L. Carbajal, C. Schimper, M. Bacher, H. Rennhofer, J.-M. Nedelec, H. C. Lichtenegger, T. Rosenau and F. Liebner, *Cellulose*, 2016, **23**, 1949-1966.
8. F. Jiang, S. Hu and Y.-l. Hsieh, *ACS Appl. Nano Mater.*, 2018, **1**, 6701-6710.
9. J. Wei, S. Geng, J. Hedlund and K. Oksman, *Cellulose*, 2020, **27**, 2695-2707.
10. H. Sai, R. Fu, L. Xing, J. Xiang, Z. Li, F. Li and T. Zhang, *ACS Appl. Mater. Interfaces*, 2015, **7**, 7373-7381.
11. Y. Li, L. Zhu, N. Grishkewich, K. C. Tam, J. Yuan, Z. Mao and X. Sui, *ACS Appl. Mater. Interfaces*, 2019, **11**, 9367-9373.